Project no. 265863

ACCESS

Arctic Climate Change, Economy and Society

Instrument: Collaborative Project
Thematic Priority: Ocean.2010-1 "Quantification of climate change impacts on economic sectors in the Arctic"

D1.24 – Integrate additional satellite sensors into daily ice drift map production to improve summer (melt season) accuracy

Due date of deliverable: **30/06/2013**

Actual submission date: **16/09/2013**

Used Person/months: **1.5**

Start date of project: **March 1st, 2011**

Duration: **48 months**

Organisation name of lead contractor for this deliverable: **Met.no**

	Project co-funded by the European Commission within the Seventh Framework Programme (2007-2013)	
	Dissemination Level	
PU	Public	X
PP	Restricted to other programme participants (including the Commission Services)	
RE	Restricted to a group specified by the consortium (including the Commission Services)	
CO	Confidential, only for members of the consortium (including the Commission Services)	

Deliverable report: D1.24 – Integrate additional satellite
sensors into daily ice drift map production to improve
summer (melt season) accuracy

Contents

Executive summary

The two main operational sea ice motion products based on low-resolution satellite images (from IFREMER and OSISAF) stop producing drift maps in the melt season months (May-September). Melting at the surface of the ice, and large atmospheric perturbations make it very challenging to retrieve quality checked vectors in that period.

We investigate several ways to supplement the current OSISAF algorithm to obtain more reliable vectors on a daily basis during summer by 1) using fields from the ERA-Interim dataset, 2) using statistical measures extracted from the satellite images, and 3) using the 18.7 GHz channels of the AMSR-E instruments.

Results obtained, especially with the AMSR-E 18.7 GHz are encouraging. But the short research effort we could conduct during ACCESS do not allow us to conclude on immediate modifications to the OSISAF processing chain that would allow reliable ice motion maps during summer.

This report summarizes our findings, and identifies possible ways forward for continuing such research in the context of other projects.

Introduction

The monitoring of Arctic sea ice motion from space has been conducted by several investigators, especially since relatively higher resolution imaging channels have been carried by satellites. Sea ice motion extraction algorithms, based on maximum correlation techniques, were first applied on Synthetic Apperture Radar (SAR, ~100m ground resolution) and Advanced Very High-Resolution Radiometer (AVHRR, ~1km ground resolution) images. They were later adapted to satellite sensors with coarser ground resolution (typically 10-20 km) such as the various scatterometers (NSCAT, QuikSCAT, now ASCAT) and passive microwave instruments such as SSM/I and AMSR-E.

A clear advantage of the latter class of satellite instruments is the possibility to cover whole basin at a daily repeat rate, allowing for following sea ice motion variability over shorter time scales than possible with SAR (due to revisit time) and AVHRR (mainly due to cloud cover). In the meantime, the coarse spatial resolution of the images prevents observation of localized dynamical features which are so important for sea ice physics, namely deformation patterns of convergence or shear.

Nevertheless, datasets such as the one distributed by CERSAT/IFREMER and, more recently, the OSISAF met a strong interest for ocean/ice modelling process studies, validation exercises, or even for routine ingestion in models via data assimilation.

Apart from not resolving fine deformation patterns in the ice pack, a strong weakness of the ice motion products based on these low-resolution satellite instruments is their un-reliability during the summer (melting) season. Both the CERSAT and the OSISAF products are halted during summer and conservative dates such as May 1st and September 30th are used to define a period of time when the retrieved vector field is so un-reliable, that it makes no sense to distribute it to users, even with enlarged uncertainties.

In this study, we take as a starting point the processing of ice motion product from the OSISAF operational chains, and investigate several directions that could lead to provide more vectors during the melt season. A first section briefly introduces the algorithms applied to generate the OSISAF ice drift product, with emphasis on the filters designed to detect "rogue vectors". The detection of these erroneous vectors is of prime importance for the quality of ice drift products all year round, while it fails during the melt season. Then, we investigate several approaches to supplement the existing filters during summer melt season. In a third section, we experiment applying the ice drift algorithm on imaging channels that are currently not used in the operational OSISAF product (mainly the 19 GHz channels), and conclude onto the potential of these to provide reliable ice drift vectors in the core of the melt season (June, July, and August). We conclude in a last section and point to future research directions.

The OSISAF low-resolution sea ice drift product

Main principles and characteristics

Ice motion tracking

The ice tracking processor implemented in the OSISAF first builds daily average maps of satellite signals. The satellite signal is either brightness temperatures for passive microwave instruments (e.g. SSM/I and AMSR-E) or radar backscatter for scatterometers (e.g. ASCAT). The specific wavelengths and polarization used for each instrument are:

- SSM/I   : 85GHz H-pol and V-pol brightness temperature

- AMSR-E   : 37GHz H-pol and V-pol brightness temperature

- ASCAT   : C-band sigma0 normalized to 40 degrees incidence angle

As in the CERSAT processor, a Laplacian filter is applied to the daily images, and the ice motion algorithm is applied on these "laplacian" images.

Based on the well known Maximum Cross Correlation (MCC) method, the Continuous MCC (CMCC, designed and applied at the OSISAF) relies on a continuous step for optimizing the components of the motion vector, located at the maximum of the cross-correlation function between a reference and a candidate image blocks. In practice, virtual image pixels are interpolated from neighbouring pixels in each candidate block. The maximum point is search for in the 2D plane of valid (dx,dy) components by a "simplex" Nelder-Mead algorithm.

The main effect of using the CMCC is the removal of the quantization noise (aka tracking noise), which has hindered the retrieval of ice motion over short time spans from the same sensors. Quantization noise is responsible for MCC vector fields to look quantized, with a poor angular homogeneity and large areas with exactly the same vector.

It is noteworthy that in the case where the instrument has both a V and a H polarization channel for a given wavelength (e.g. AMSR-E 37GHz H- and V-pol Tb), the strategy adopted in the OSISAF is to maximize the sum of two cross-correlation function (a H and V one) rather than retrieving two independent vector fields and merging them a-posteriori.

Filtering steps

As with all motion tracking algorithm, the raw vector field resulting from applying the CMCC must be filtered for untrustworthy vectors before delivery to the users. The main issue is the presence of erroneous, *aka* rogue vectors, which strongly differ -in both direction and magnitude- from the locally surrounding motion field. The reason for these rogue vectors is usually noise in one of the start or stop images, that blur the shape of the cross-correlation function and shifts the location of its maximum. It can also happen that events on the surface of sea ice (snowfall, melting, etc…) radically change the image recorded at a given location, and prevent any matching of image pattern. These rogue vectors are fortunately not many, and strategies can be designed to detect and correct them.

In the OSISAF processing chain, the original "level0" ice motion fields obtained from applying the CMCC at each product grid location are first filtered by a local consistency filter (to detect and correct rogue vectors). The "level1" ice motion field is subsequently processed through a maximum cross-correlation threshold filter to remove additional vectors that are untrustworthy. The resulting "level2" fields are later formatted into the final OSISAF product.

The local consistency filter computes, for each "lev0" (central) vector, the average drift vector from its 8 surrounding vectors. If the drift estimated at the central vector differs too much from the local area average drift, it is identified as a rogue vector. Instead of discarding the vector, a correction step is attempted where the CMCC is applied once more, but with a constraint radius (several tens of kilometre) around the local average drift. It is very often that a valid maximum of cross-correlation can be identified in the vicinity of the local average drift. This new vector is a "corrected" version of the rogue vector that can be inserted in the product grid before the next rogue vector is searched for in the "lev0" field. To function, this filtering step requires a minimum number of neighbours for each vector. Consequently, isolated "lev0" vectors that are processed close to the coast or in the many straits of the Canadian Arctic Archipelago have to be discarded since they cannot be validated by their neighbours.

This local consistency filter is a key part of the OSISAF ice motion processing chain, and useful motion fields can be distributed to users only because this step works. When the filter stops being able to detect all rogue vectors from a motion field, this motion field cannot be distributed to users because it may contain undetected un-trustworthy vectors. A mal-functioning filter is the main reason why the current OSISAF product cannot be distributed during the melt season.

Challenges in the melt season

During the summer melt period, several factors contribute to the failure of the motion extraction algorithms described above.

All motion extraction routines based on sequence of images rely on the hypothesis that the main change from a "start" sea ice image to the "stop" image is mainly due to motion. A second strong hypothesis is that there are some image features to track, that the images are not uniform. During the melt season, these two hypotheses are strongly challenged for the satellite imaging channels we use in the OSISAF products.

Surface melting events modify the image so radically, that the main change between two images is no more explained by motion, but by changes in the structure of the surface emitting layer (snow + ice). It is then impossible to detect motion at these melting locations. It is noteworthy that the depth of the surface emitting layer varies with the wavelength of the imaging channel. It is deeper for lower frequencies, so that an image based on the 19 GHz channels will probably be more stable during a limited melt event, than a 37 GHz image or one from 85 GHz channels. Snowfall is another element that can drastically modify images of the ice surface over short period of time, and all imaging channels are perturbed.

The second issue during summer melt is the opacity of the atmosphere. Sea ice retreat, combined with changes in the layering structure of the atmosphere at lower latitudes allow

for large quantities of atmospheric water vapour, and more humid cloud systems to enter over sea ice. These wetter (and warmer) atmospheric layers blur the signal emitted from the ice surface, to the point when it is no more possible to see details of the surface through the atmosphere. In these conditions, the changes between two images are no more a signature of motion of the ice surface but, at best, of the motion of the atmospheric features travelling over sea ice. Here again, the lower frequency channels are less contaminated by the content of the atmospheric layers: C-band sigma0 are not sensitive to changes in the atmosphere, and 19 GHz channels are less perturbed than 85 GHz.

As noted above, the detection of rogue vectors from a vector field is a key aspect of motion tracking. However, such filters only succeed when a few (1 to 3) rogue vectors are surrounded by an otherwise smooth motion field. The quality of the local area drift is crucial for detecting the untrustworthy vectors. If a large area of the motion field is covered with erroneous vectors, pointing in all directions, the local consistency filter might validate some 4-5 neighbouring vectors that are not indicating true ice motion but are by chance pointing in the same direction.

The lack of control we have on the efficiency of the filtering step during the melting season (when large area of the vector fields are covered by erroneous, randomly pointing vectors), is the reason why we choose to conservatively halt distribution of the product from May to October.

Figure 1 shows four examples of ice motion fields valid from 25th to 27th May 2008, which is well into the melting period when the OSISAF ice motion products are no more distributed to users. The top row (a,b) are processed from the SSM/I 85 GHz channels, while the bottom row are from the AMSR-E 37 GHz channels. Left column exhibits un-filtered vector fields (level0) while the maps in the right hand side column are the motion fields obtained after all the filtering was applied (level2). Both in (a) and (c), a fair number of rogue vectors can be detected. Some appear isolated in regions where the ice motion is generally well characterized by the product, while others are grouped, over a large region north of Alaska and Canada. As expected, the isolated rogue vectors are usually well detected and corrected by the filters, as can be seen from maps (b) and (d). However, the rogue vectors that are in large aggregates are not totally removed, and some groups are still visible in the filtered motion field. There is generally less rogue vectors in the motion field computed from AMSR-E channels (c) than from the SSM/I channels (a), indicating that the 37 GHz images are less affected than the 85 GHz images by the conditions prevailing above and at the surface of the ice during these two days.
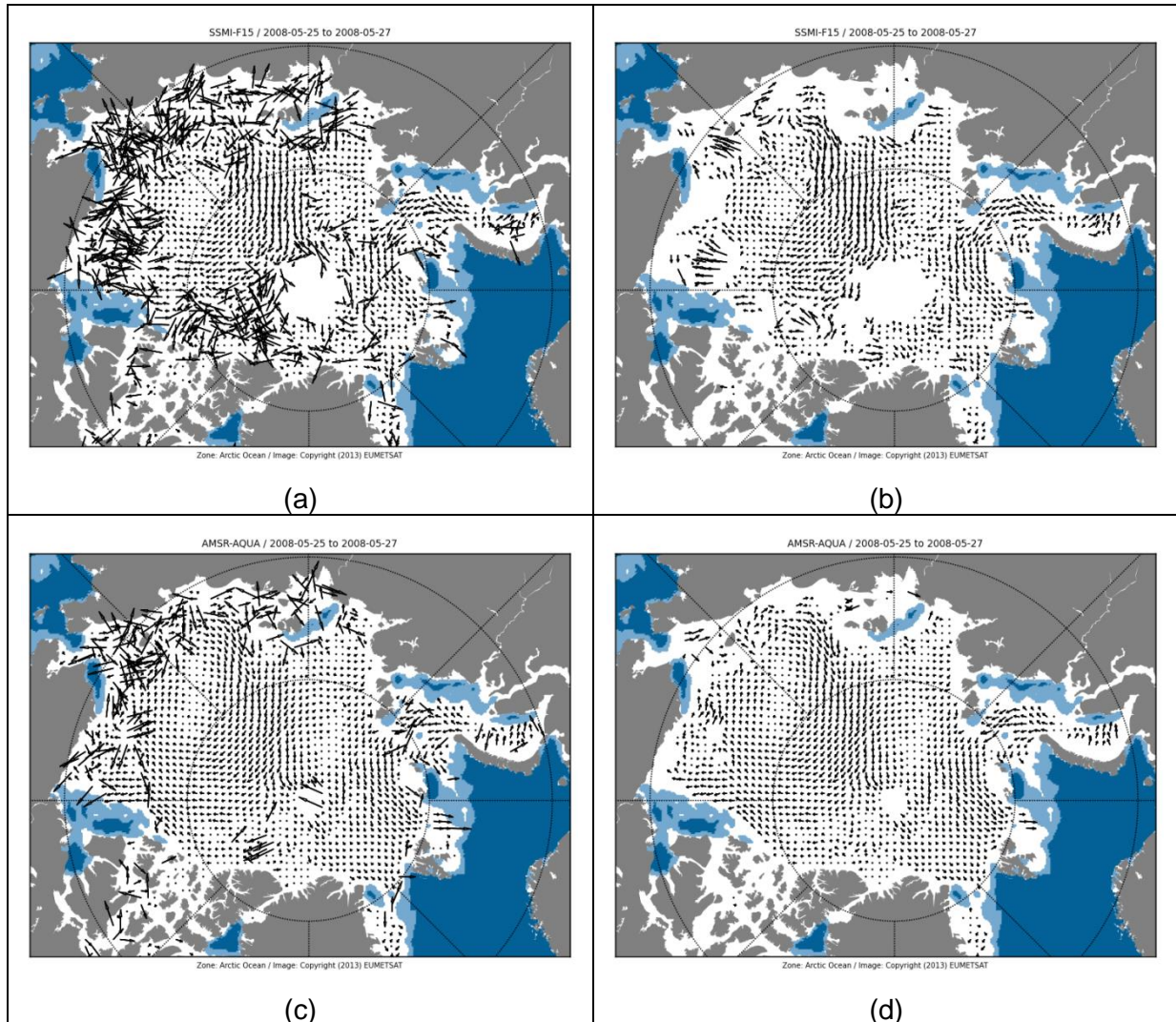
Figure 1: Examples of un-filtered (a,c) and filtered (b,d) Arctic ice motion field from 25th to 27th May 2008, as processed by the OSISAF algorithm using SSM/I F15 85GHz (a,b) and AMSR-E 37GHz (c,d) images.
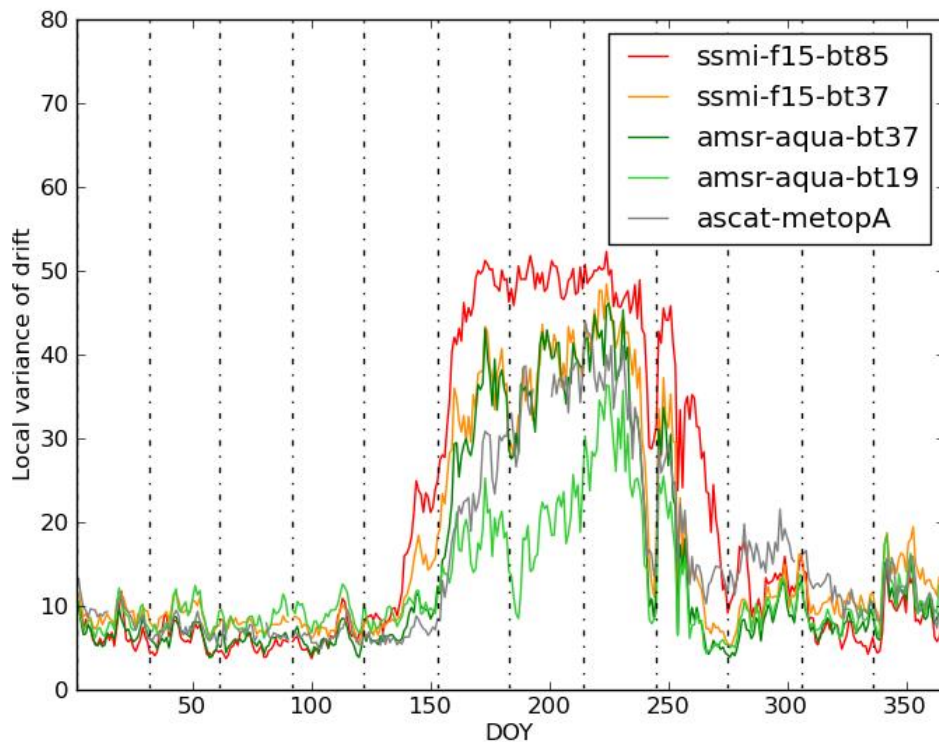
Deliverable report: D1.24 – Integrate additional satellite
sensors into daily ice drift map production to improve
summer (melt season) accuracy

Figure 2: Time series of mean local variance of unfiltered drift vectors (units km) for year 2008 over the Northern Hemisphere. Each solid line corresponds to an ice motion product computed with the OSISAF algorithm and using different imaging channels. Dashed vertical lines indicate months.

We define a measure of local variance of the vector field to monitor when the local consistency filter might work or not. The Local variance of drift V is computed as V = sqrt(Var(dX) + Var(dY)) where the variance is computed on a 3x3 neighbourhood of each valid drift vector (dX,dY) in the "lev0" field. It has unit km. On each date, the map of V indicates areas where the local consistency filter might work (low values of V) and where it probably will fail (high values of V). Figure 2 plots the time series of the daily mean (over the product grid) of the local variance of drift for selected single-sensor OSISAF products using SSM/I 85GHz channels (red), AMSR-E 37GHz channels (dark green) and ASCAT C-band sigma0 (grey). In addition, two experimental ice drift products using the same algorithm, but processing SSM/I 37 GHz channels (orange) and AMSR-E 18.7 GHz channels (light green) are included for comparison.

Before looking any further into the solid lines of Figure 2, it must be noted that they plot the mean of V over the whole Northern Hemisphere grid, and that the mean value hides a wide variability of V over such a domain. Figure 3 plots histograms of V for SSM/I 85GHz product on April 1st (left) and July 1st (right). Since this plot (and Figure 2) is made from "lev0" products, before any attempt of the local consistency filter to detect rogue vectors, it is not a surprise to find a small number of grid locations with high value of V even in the April 1st example. These locations can correspond to isolated rogue vectors or to larger groups of them in Arctic peripheral basins such as Hudson and Baffin Bay. Indeed, at that time of year,

the Central Arctic might still be in winter conditions while sea ice at lower latitudes is entering its melt season.
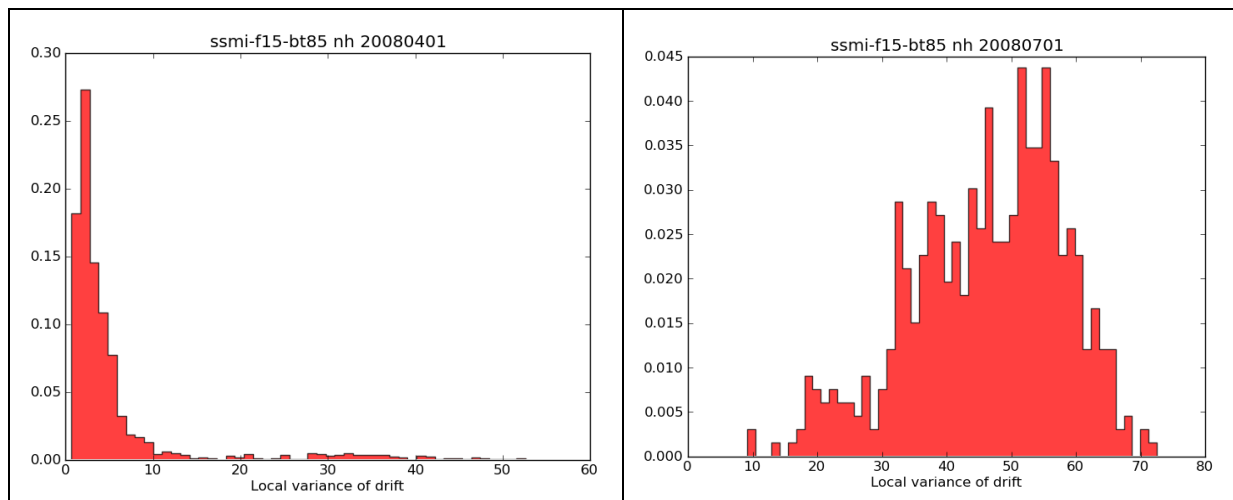

Figure 3: Histogram of local variability of drift, V, over the Northern Hemisphere grid for the SSM/I 85GHz single-sensor product on April 1st (left) and July 1st 2008 (right).

The seasonal cycle in Figure 2 reveals that all single sensor products show low values of V during the period where the products are distributed, from Jan 1st to April 30th and from Oct 1st to Dec 31st. Values of V are much higher during the core of summer melt season (June throughout September), for all of the products, indicating that the local consistency filter will be challenged in this period, whatever the input imaging channels are used. Of all the products tested, the one using AMSR-E 18.7 GHz gives best results during the core of summer.

The transition months (May for early melting and September for early freeze-up) are maybe the most interesting periods since there seems to be a potential for pushing the current limit dates, at least for some area of the product grid, and for some of the single-sensor products. For example, the two AMSR-E ice motion fields and the one from ASCAT seems to perform quite well all the way through June 1st, while only the AMSR-E products and the SSM/I 37GHz product are ready to be used by September 15th.

In the next section, we will discuss ways to get trustworthy drift information during these transition months by use of additional information.

Towards Arctic wide ice drift information in melt season

Use ERA-Interim re-analysis

The ERA-Interim atmosphere re-analysis available from ECMWF is documented on (http://www.ecmwf.int/research/era/do/get/era-interim). We access 3-hourly fields and remap them to the same projection and grid that is used for the OSISAF ice drift, with 62.5 km spacing (original resolution is about 0.7 deg). From these 3-hourly maps, we compute maps of the average of Total Column Water Vapour (TCWV), the average Total Cloud Liquid Water

Deliverable report: D1.24 – Integrate additional satellite
sensors into daily ice drift map production to improve
summer (melt season) accuracy

(TCLW) and Total Cloud Ice Water (TCIW). The averaging period runs from the start-day of the drift product (at 00utc) to the stop-day of the drift (at 23:59 utc). For each vector in each drift product map, we thus obtain a 36 hours average of TCWV, TCLW, and TCIW. These 3 variables strongly influence the opacity of the atmospheric layers. In addition, we also compute an integrated degree-hour quantity based on Temperature at 2m height (T2M).

$$\text{DegHours} = {}_0\!\int^{36} \mathbb{1}(T2m(h) - 273.15)*(T2m(h) - 273.15)\ dh$$

In cases where the whole T2m time series is under 273.15 K, DegHours is 0. If the time series oscillates both over and under 273.15 K, the part of the curve that lies under the threshold do not compensate for the part which is above the threshold. DegHours (unit Celsius.hours) is thus an integrated measure of the amount of positive degrees available in the air to melt the sea ice surface.
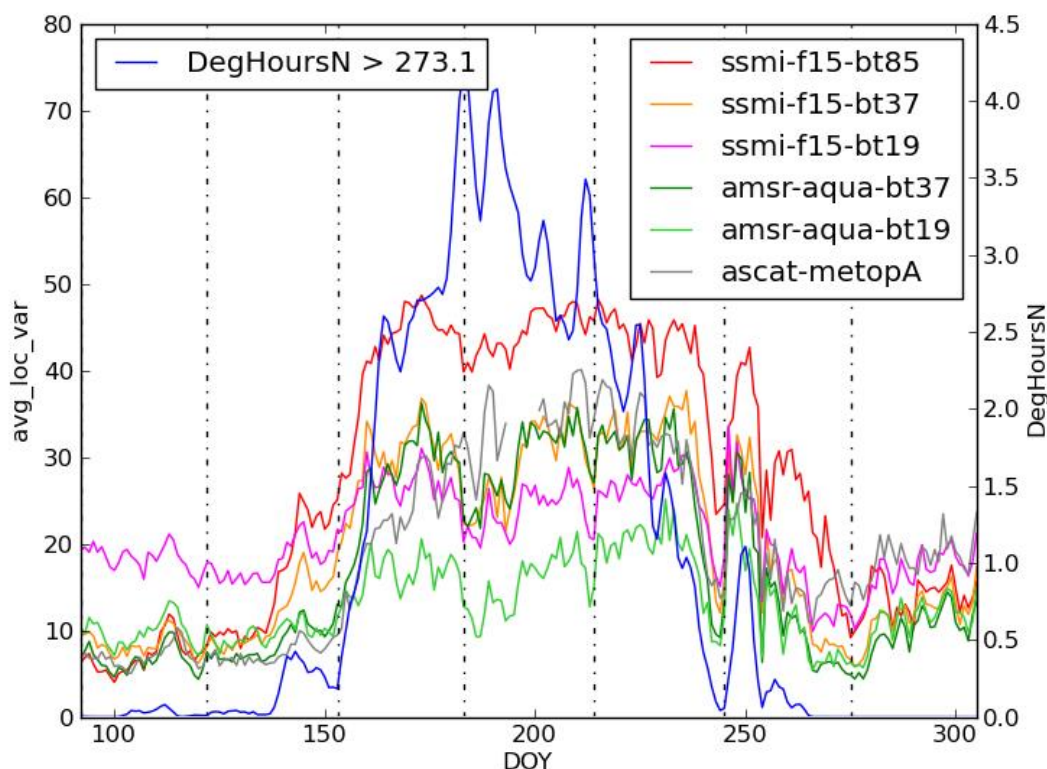

Figure 4: Same as Figure 2 but with time series of DegHours (blue) added, and zoomed on 1st April to 31 October 2008

Figure 4 overlays a time series of (map averaged) DegHours (blue solid line) on the time series of local variance of drift V already displayed in Figure 2 (page 9). It appears clearly that the variations of DegHours are quite correlated to those of V, especially in the transition moths of May and September. Note the co-varying bumps from DOY 140 to 160, and around DOY 250. During the core of the summer season, there does not seem to be obvious correlation between the curves of V and the one of DegHours.

In order to better understand if fields from ERA-Interim can help localize regions where the ice motion algorithm might fail, we plot 2D histograms of local variance of drift V (x axis) and

the 4 time-integrated ERA-Interim variables described earlier (that are DegHours, TCWV_AVG, TCLW_AVG, TCIW_AVG).
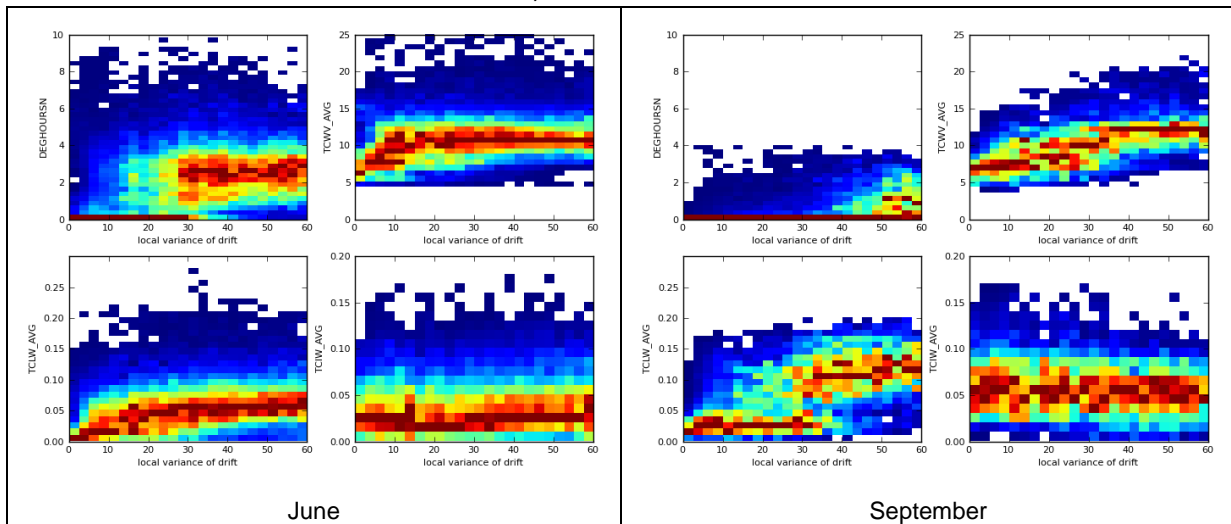

Figure 5: Example 2D histograms of V (x-axis) against the 4 selected ERA-Interim variables (y-axis) for the AMSR-E 37 GHz product in June and September 2008. The histograms are normalized along the x-axis so that each column has max value of 1.

Figure 5 represent such histograms for the AMSR-E 37 GHz ice drift product, in June and September (all other imaging channels and months are in annex to this report, Figure 15 to Figure 21). We recall that high values of V (say V > 20) are those where the ice motion algorithm fail, since the drift field looks very random around such locations. According to the histograms, a low threshold on DegHours (e.g. DegHours > 0.01) could identify many of the erroneous regions for AMSR-E 37GHz in June. This ERA-Interim variable is however not going to help in September when most locations have DegHours of 0. In September, TCLW might be of greater help to screen out areas where the motion algorithm will fail (e.g. TCLW_AVG > 0.06). The TCIW quantity does not seem to help in either months, either because TCIW does not influence so much the AMSR-E 37 GHz imaging channels, or because the TCIW found in the ERA-Interim dataset (at very high latitudes) are not accurately matching the amount of atmospheric ice water at this time of year.
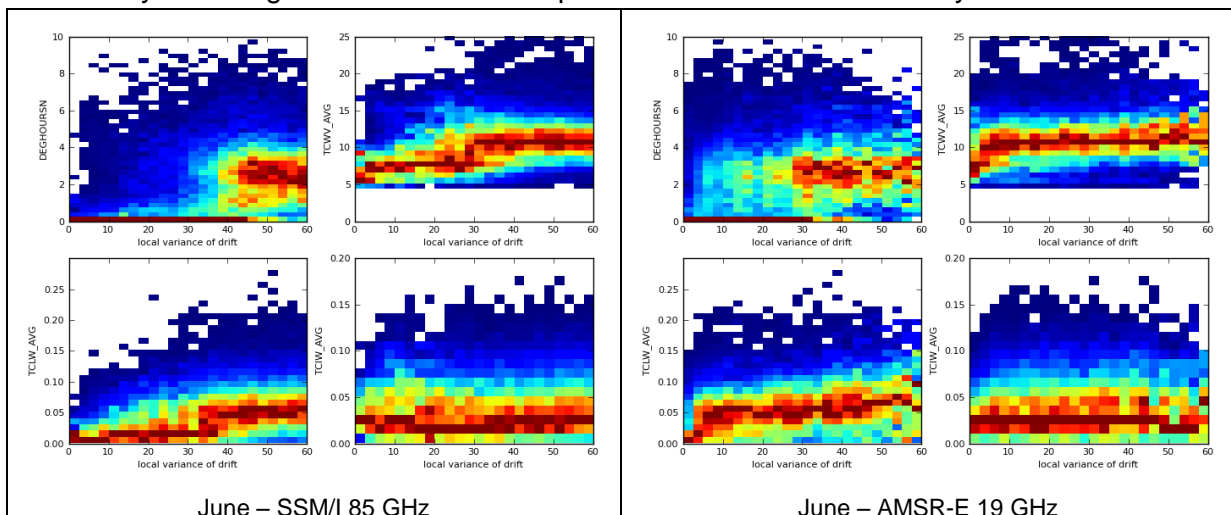
Figure 6: Same as previous but for SSM/I 85 GHz and AMSR-E 19 GHz in June.

Analysing the DegHours graphs on Figure 5 and Figure 6 reveals that an approach with a unique threshold would probably not work optimally. While a threshold of 0.01 on DegHours would remove only "bad" vectors for SSM/I 85 GHz (Figure 6 - left), it would remove a non-negligible amount of potentially interesting vectors (cyan colour in the range V < 20) for AMSR-E 37 GHz (Figure 5) and even more so for AMSR-E 19 GHz (Figure 6 - right).

Use statistics from sequences of satellite images

Conversely to the physical variables contained in ERA-Interim, the satellite images we use in ice motion tracking are only Brightness Temperatures (Tb) or backscatter values in various wavelengths. They thus sound less interesting for characterizing events such as optically thick atmospheric layers, or surface melting that both might prevent success of ice motion retrieval. The images only contain the complex superposition of signatures from surface and atmosphere, which impact the images differently at the different wavelengths and polarization. On the other hand, the images are those directly used for tracking ice motion, and are thus "the truth", in the sense that they are not biased like a T2m might be or mis-located like a TCLW feature might be in ERA-Iterim fields.

It is thus interesting to see if an analysis of the satellite images, both in terms of spatial and temporal variations can help characterize locations where the motion extraction routine will fail. For this purpose, we plot 2D histograms of the local variance of drift against various statistics we extract from a sequence of SSM/I (19 GHz H+V), (37 GHz H+V) and (85 GHz H+V). The reason we limit this analysis to SSM/I instruments is because it has the 3 main channels we can use to track ice motion all year long (like AMSR-E has), and because we know we have access to SSM/I data everyday in the "satellite era" (since 1992 with 85 GHz).

The following image statistics are studied in relation to the local variance of the drift:

- Avg : local average (120x120 km) of the satellite image, on start day of the drift;

- Minstd : minimum of the local average of the satellite image on start day and of the same quantity at the end day of the drift;

- SumDstd : Standard deviation of the image during the 24 hours of gridding/compositing, summed over the 3 days of the drift period;

- Rat : ratio between Avg on start day of the drift and Avg on the stop day of the drift.

Avg is a measure of the Tb level for each channel. For a given surface emissivity, air temperature, water content and all other atmospheric variables contribute to changes in the Tbs in the different channels. One can expect a general increase of Tb with increasing atmospheric influence, and Avg is thus meant for an indication of atmospheric perturbation.

Minstd is meant as an indication of the strength of the local variation in the sub-image that will be used for tracking sea ice. Intuitively, higher Std mean more contrast in the image and thus better ability for motion tracking. Areas with very low Std might not contain enough structures to allow for successful motion tracking.

SumDstd is an indication of the variation of the satellite signal over one location, during 24 hours, summed over the 3 days of the drift perdiod. Since weather patterns travel faster than sea ice, higher values of Dstd could indicate weather-induced changes in the image. But image geo-location and sub-daily drift in highly dynamic region also give a higher SumDstd.

Finally, Rat (ratio) is an indication of how the images change in level during the drift period. Since, 1) the OSISAF ice tracking algorithm is applied on Laplacian-filtered images, which effectively normalize the images in both level and standard deviation, and 2) the cross-correlation metric used for matching the sub-images is not sensitive to changes in the intensity, the change in intensity measured by Rat is something overlooked by the tracking algorithm. Dramatic changes in the intensity of the images could be related to dramatic changes in the surface and/or weather situation, and is thus interesting to look at in relation to local variance of drift.
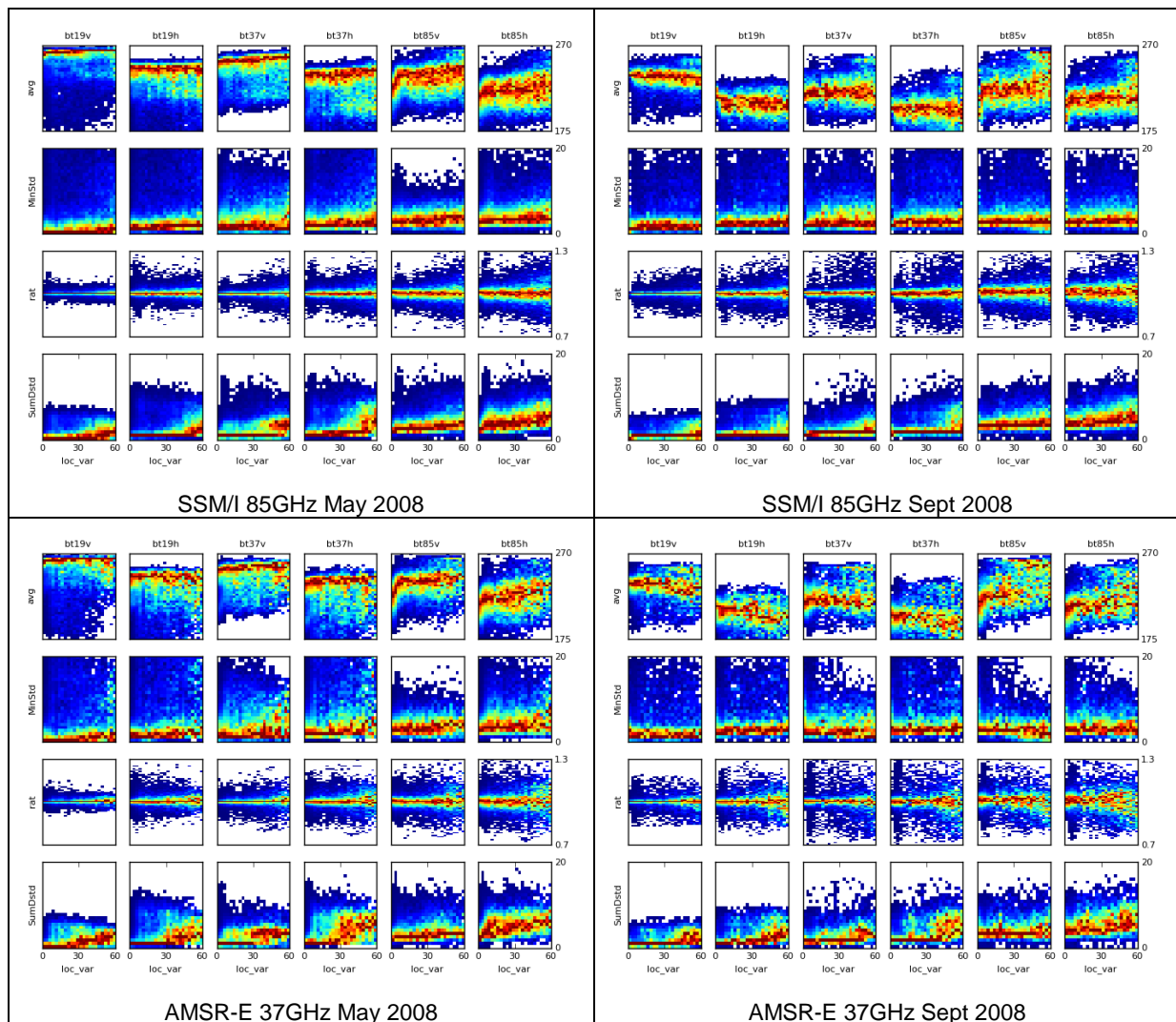
Figure 7: 2D histograms of local variance of drift (x-axis) against 4 statistical measures of variation in SSM/I satellite images for May and September 2008.

Figure 7 displays variations of the 4 statistical measures introduced earlier against the local variance of drift fields.

It reveals that the Rat measure (3rd row) might be interesting to investigate further since departure from Rat=1 occurs mostly at high-values of the local variance of drift. This is especially true for the Rat measured from the high-frequency channels of SSM/I. The other statistical measures are somewhat more difficult to use. It seems the level of Tb 85GHz (especially V-pol) (1st row) could be used at least in May: the majority of vectors (both from AMSR-E 37GHz and SSM/I 85GHz) with high local variance of drift also have rather large values of Tb 85GHz and it might be possible to find a threshold that separates the two categories. Such a feature is much less obvious in September. Finally, there might be interesting information in the SumDstd of Tb 37Ghz (mostly H-pol). Vectors localized with high sub-daily variations of Tb 37Ghz exhibit much higher local variance than the others.

Sea-ice drift during the core of summer melt season

As can be deduced from Figure 4, most of the ice drift products fail during the core of summer, since they have very high values of averaged local variance of drift. The drift product obtained from the AMSR-E 19GHz channels seems the most promising (light green solid line).

Sea ice motion vectors have already been successfully extracted from these channels by Ron Kwok (GRL, 2008). We are thus not surprised that they show some ability here. This is also illustrated in the monthly histograms of local variance of drift (Figure 8 to Figure 14). AMSR-E 19GHz is the product showing fewest randomly pointing vectors in the core of summer (but significantly more than others during the April and October months).

Although it shows potential, the issue is the same as with the "Winter" ice drift products in the transition periods. The challenge is always to separate the good from the rogue vectors using additional information than just the drift field.

Conclusion and way forward

There are two main factors that challenge the retrieval of sea ice motion during the summer melt season. The first of them is that the changes observed in satellite images are not any more related to motion of the ice, but also to abrupt changes in the surface emitting layer of the snow and ice (melting) and/or the signature of atmospheric features, mainly larger water content. The second challenge is that the drift field obtained from the classic cross-correlation method is very noisy and exhibit large occurrence of rogue vectors, vectors pointing in seemingly random directions. The detection of these rogue vectors is mostly not an issue during winter because they are isolated. But their gathering in bigger groups during summer makes it very difficult to detect and remove them from the map.

We investigated two ways for detecting these rogue vectors using additional information than just the ice motion field: importing ERA-Interim fields, and looking at statistical measures of image changes that are not taken into account by the drift algorithm.

Both these approaches showed limited success.

Most of the features we studied could be related somewhat to the local variance of drift (our measure of how random the ice drift field looks like), but there was no easy way to transform these relationship into thresholds and test cases that could for sure separate good vectors from good ones.

Ice drift from the 18.7 GHz channels of AMSR-E seems the only way forward for obtaining vectors in the core of summer, but unfortunately it is there also quite challenging to separate the good from the bad vectors.

This research effort nevertheless points towards several new ideas that will be tested in the future:

- Taking into account the change of image intensity as part of the motion tracking algorithm;

- Adopt a more conservative strategy during summer and remove rogue vectors (instead of trying to correct them as we do now during summer).

- Build a small ensemble of drift products every day, from perturbed satellite images. Location with high variability in the ensemble would be marked as non-reliable and removed from the product grid.

Research to obtain more reliable ice motion vectors during summer will be continued in the frame of the EUMETSAT Ocean and Sea Ice Satellite Application Monitoring (OSISAF), tentatively in 2015-16.

ANNEXES

Deliverable report: D1.24 – Integrate additional satellite
sensors into daily ice drift map production to improve
summer (melt season) accuracy

Monthly histograms of V

April 2008
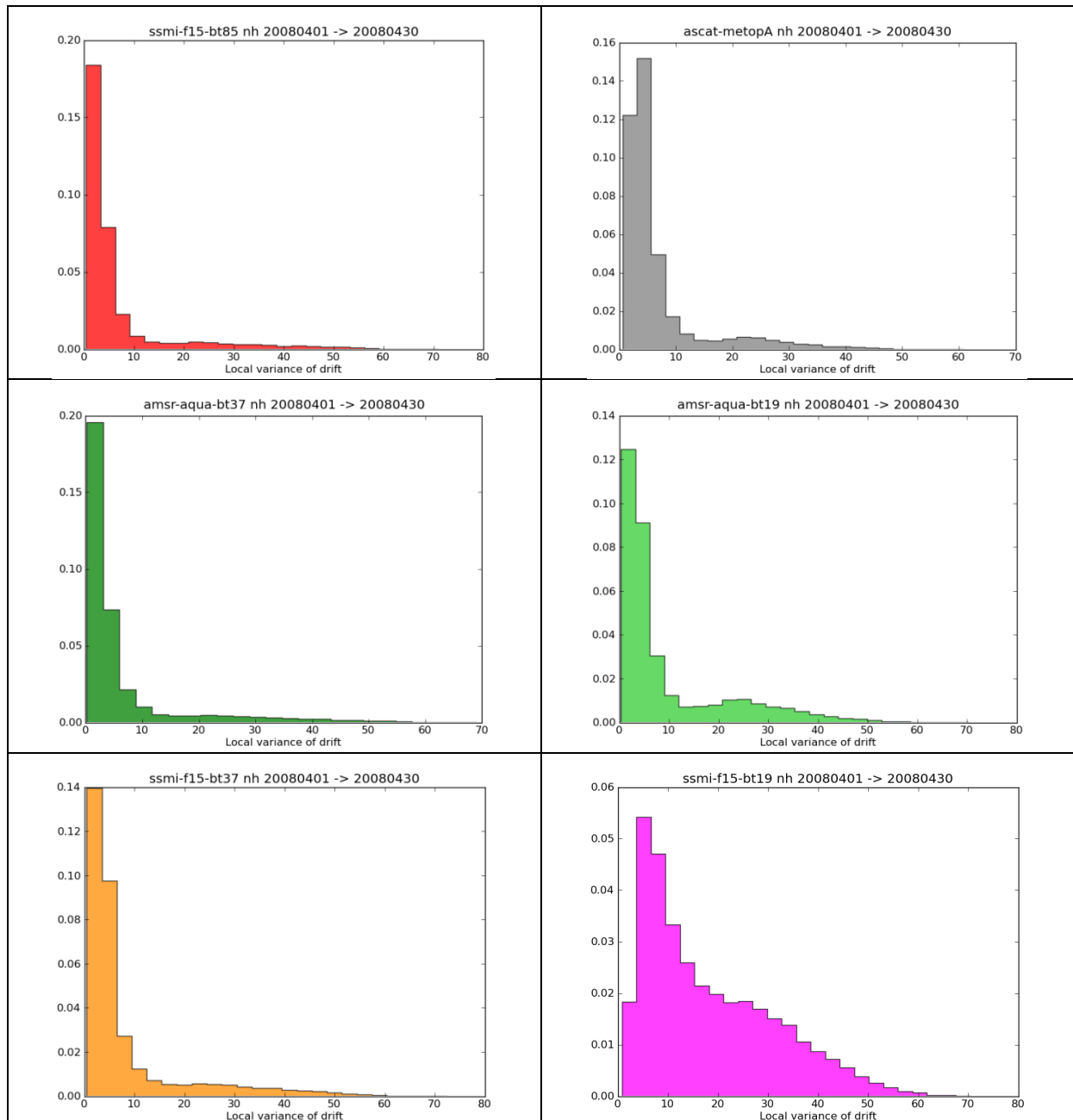
Figure 8: April monthly histogram of V (local variance of drift) for SSM/I (85GHz), ASCAT (C-band), AMSR-E (37GHz), AMSR-E (19GHz), SSM/I (37GHz) and SSM/I (19GHz) ice drift products
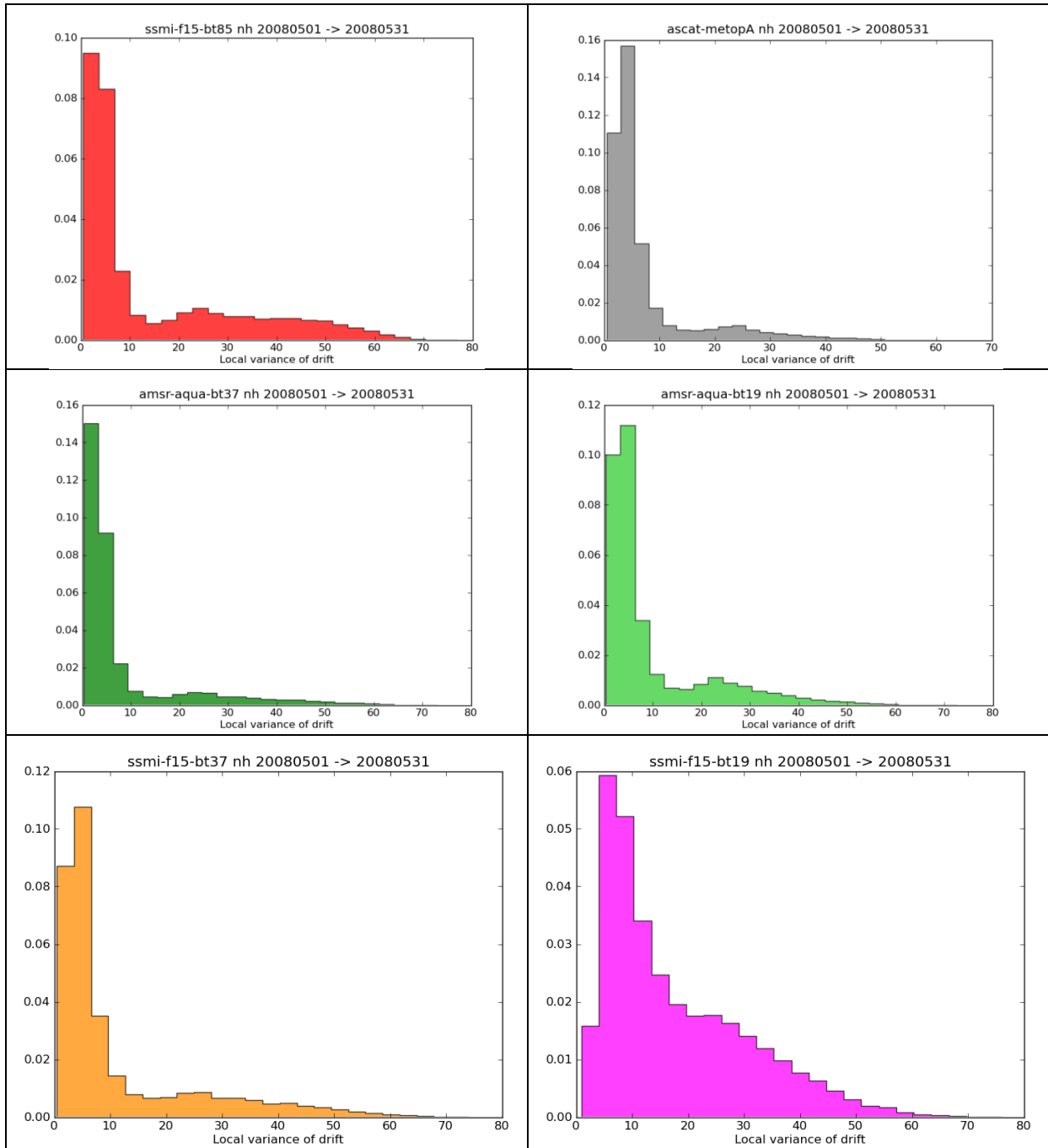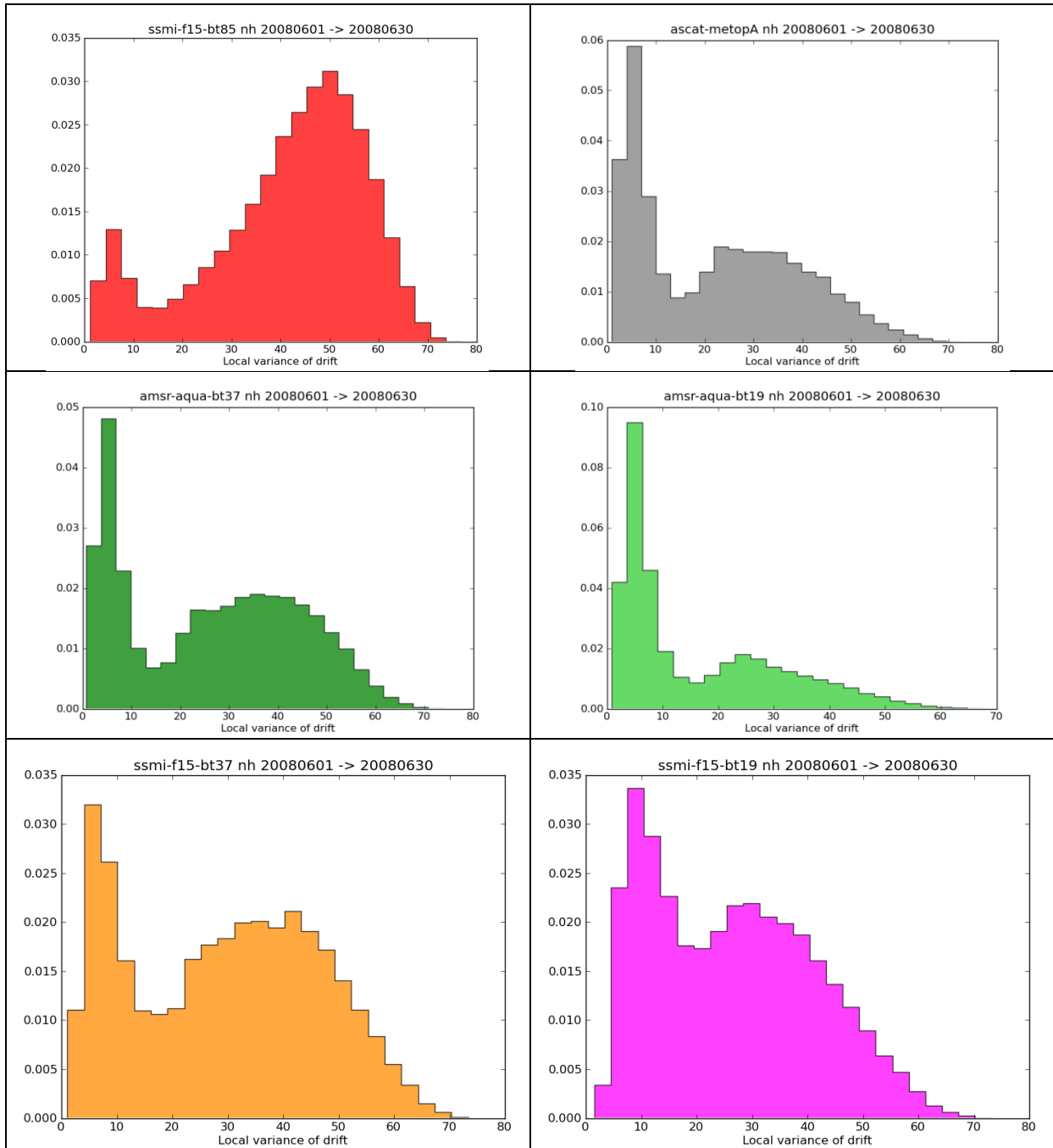
May 2008

Figure 9: Same as previous for May

Deliverable report: D1.24 – Integrate additional satellite
sensors into daily ice drift map production to improve
summer (melt season) accuracy

June 2008

Figure 10: Same as previous for June

July 2008
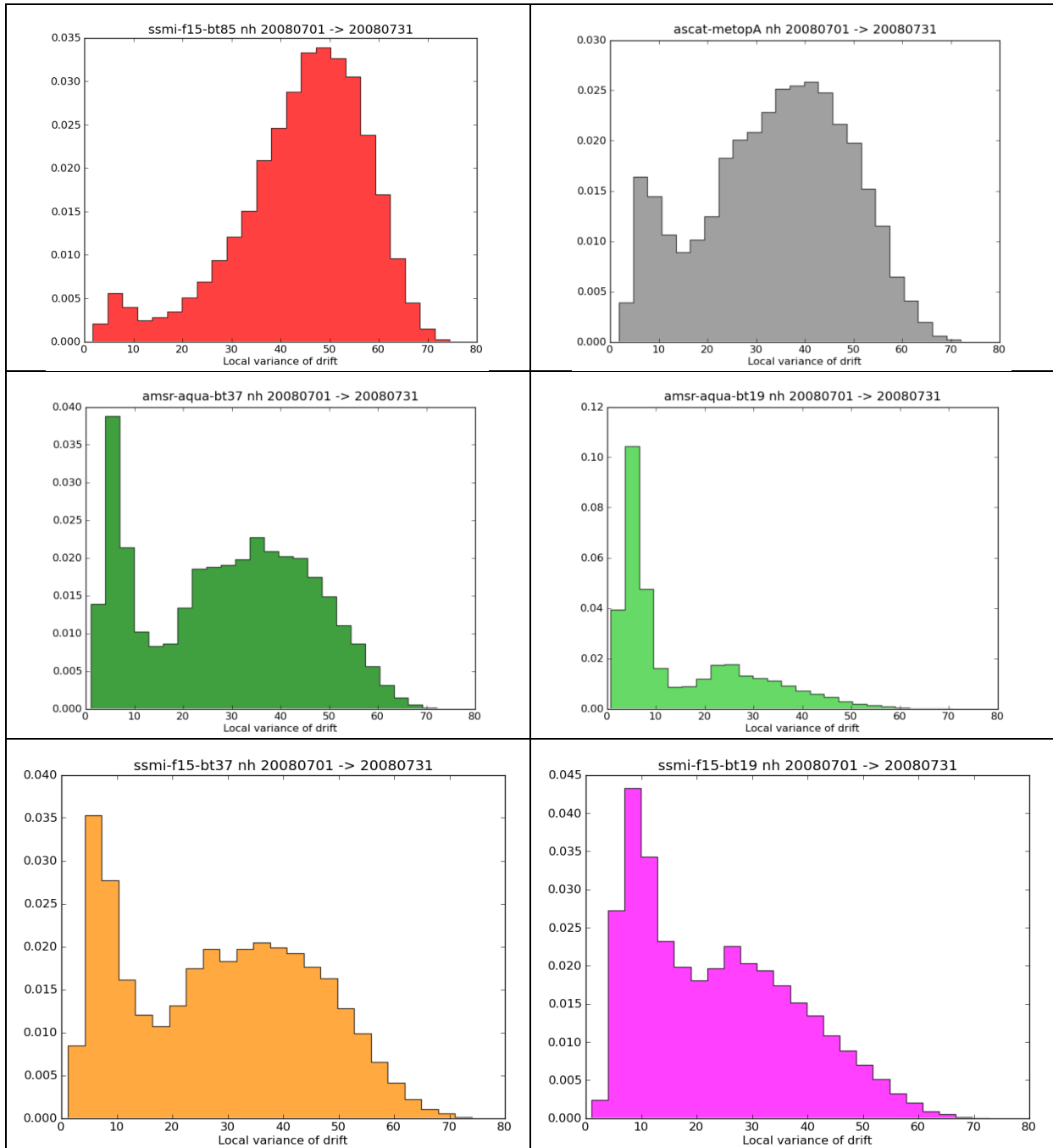
Figure 11: Same as previous for July

August 2008
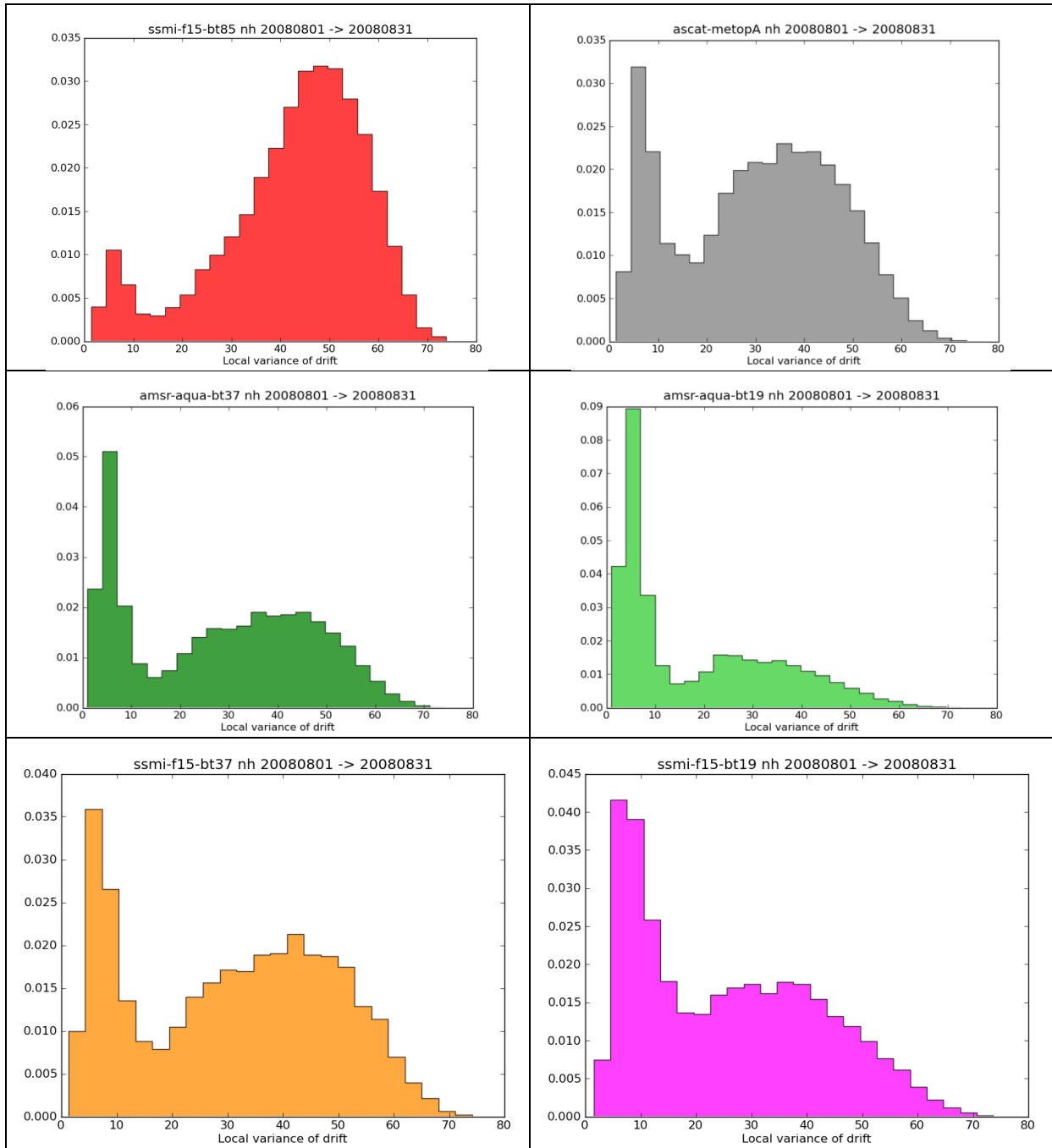
Figure 12: Same as previous for August

Deliverable report: D1.24 – Integrate additional satellite
sensors into daily ice drift map production to improve
summer (melt season) accuracy
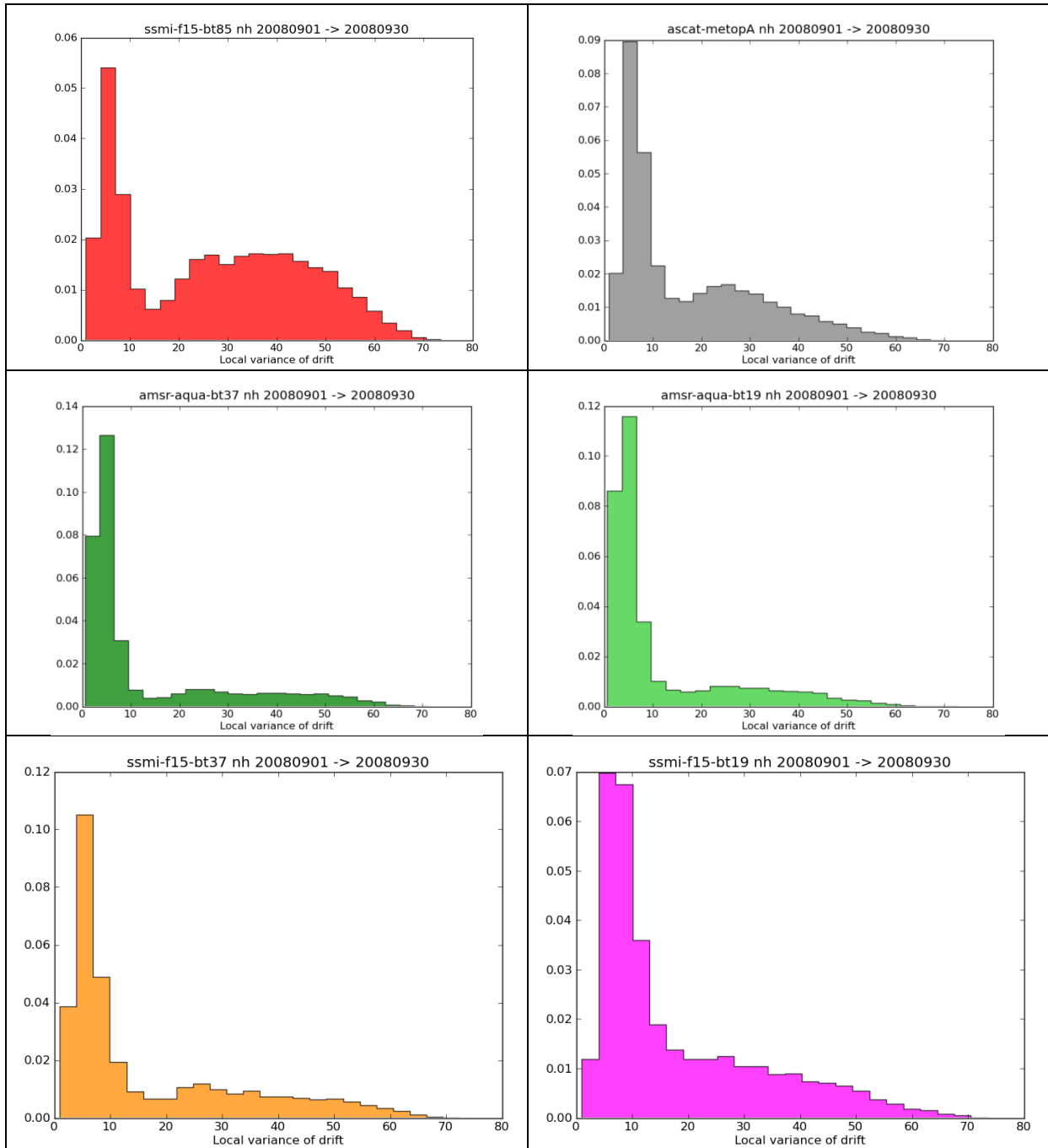
September 2008

Figure 13: Same as previous for September

October 2008
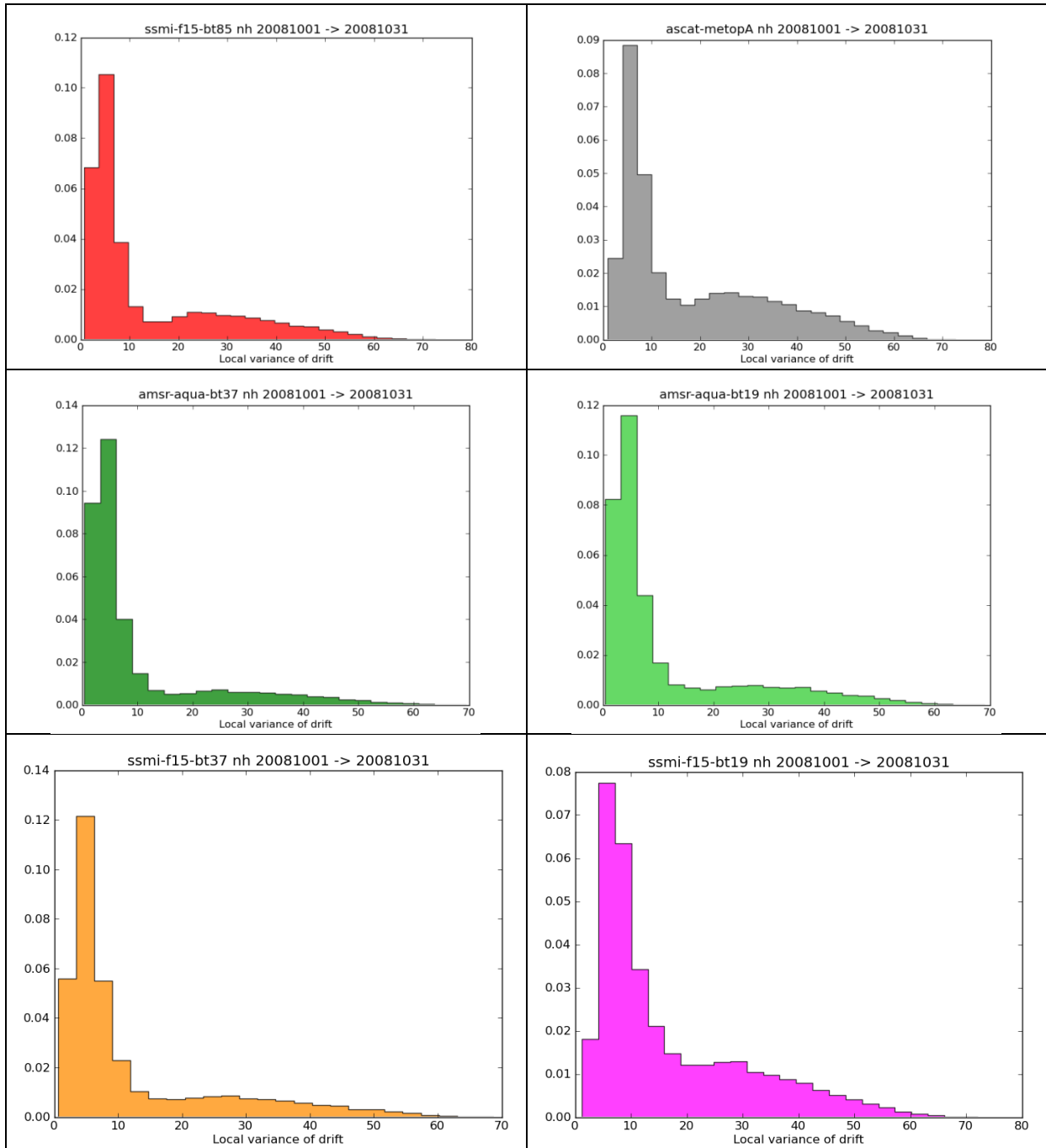
Figure 14: Same as previous for October

Monthly 2D histogram of V against ERA-Interim fields

April 2008
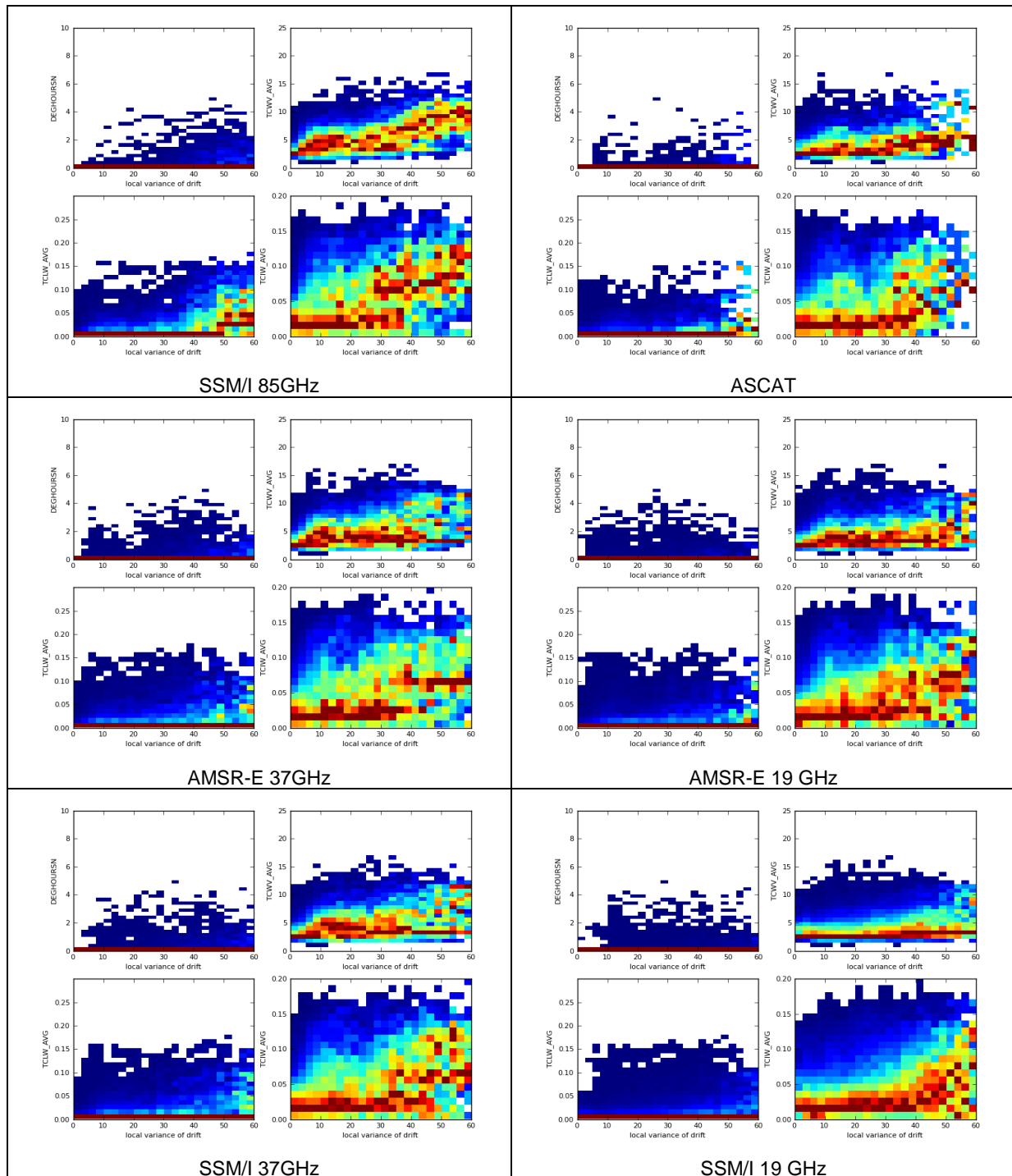
Figure 15: 2D histogram of local variance of drift V (x-axis) against selected ERA-Interim parameters (y-axis) for 6 ice drift products. The histograms are normalized along the x-axis, so that each column has a max value of 1.
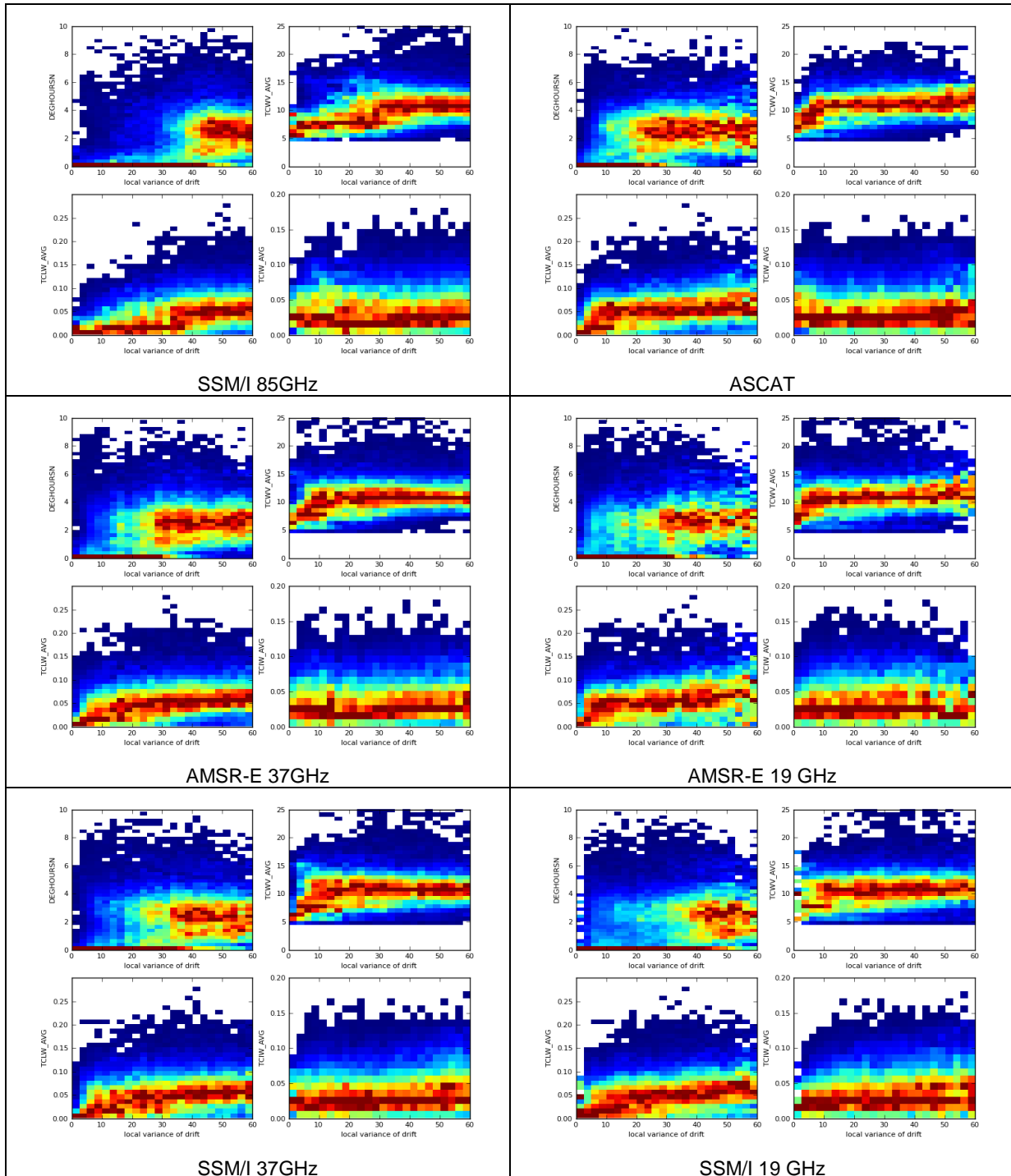
May 2008
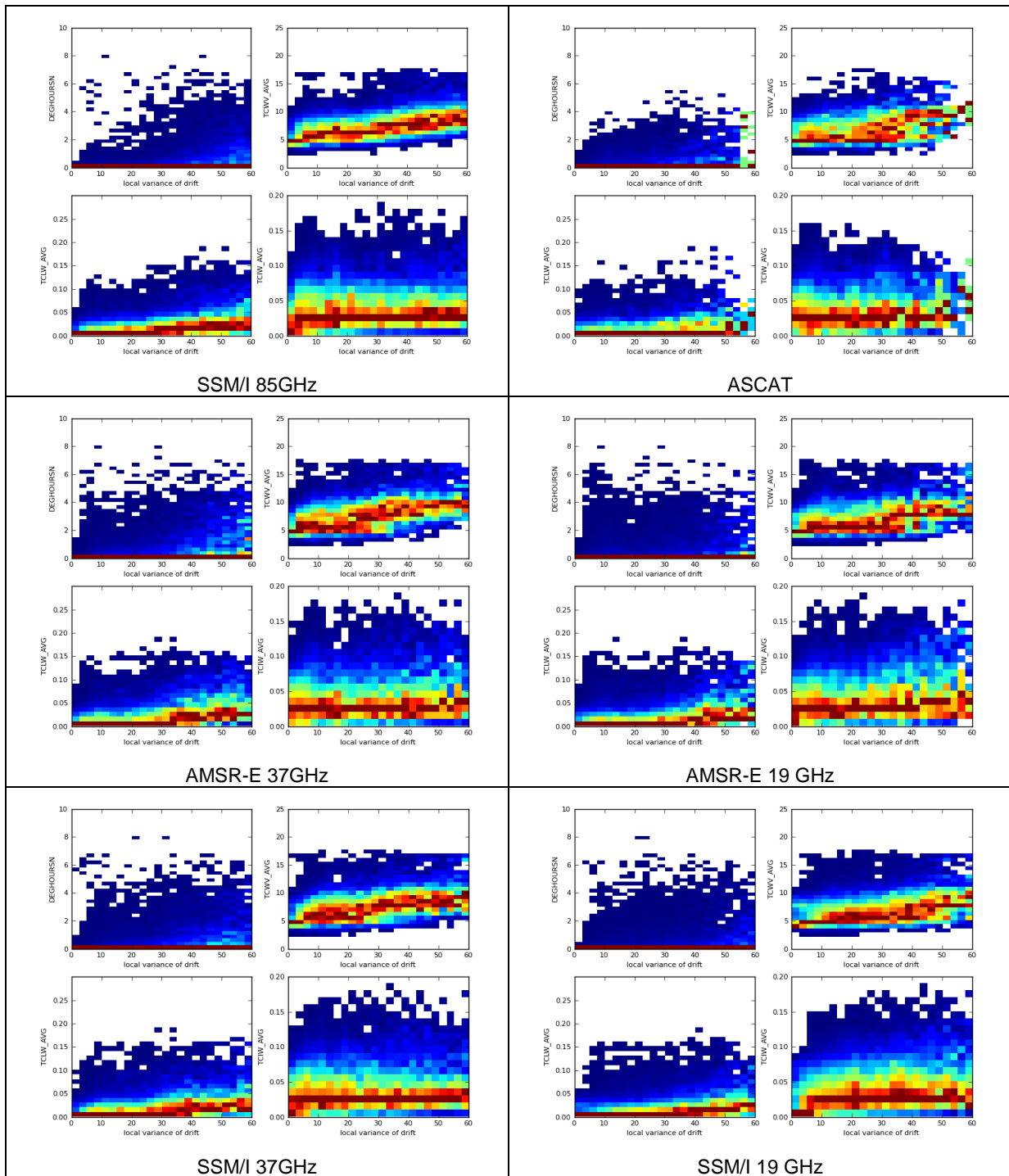
Figure 16: same as previous for May

June 2008

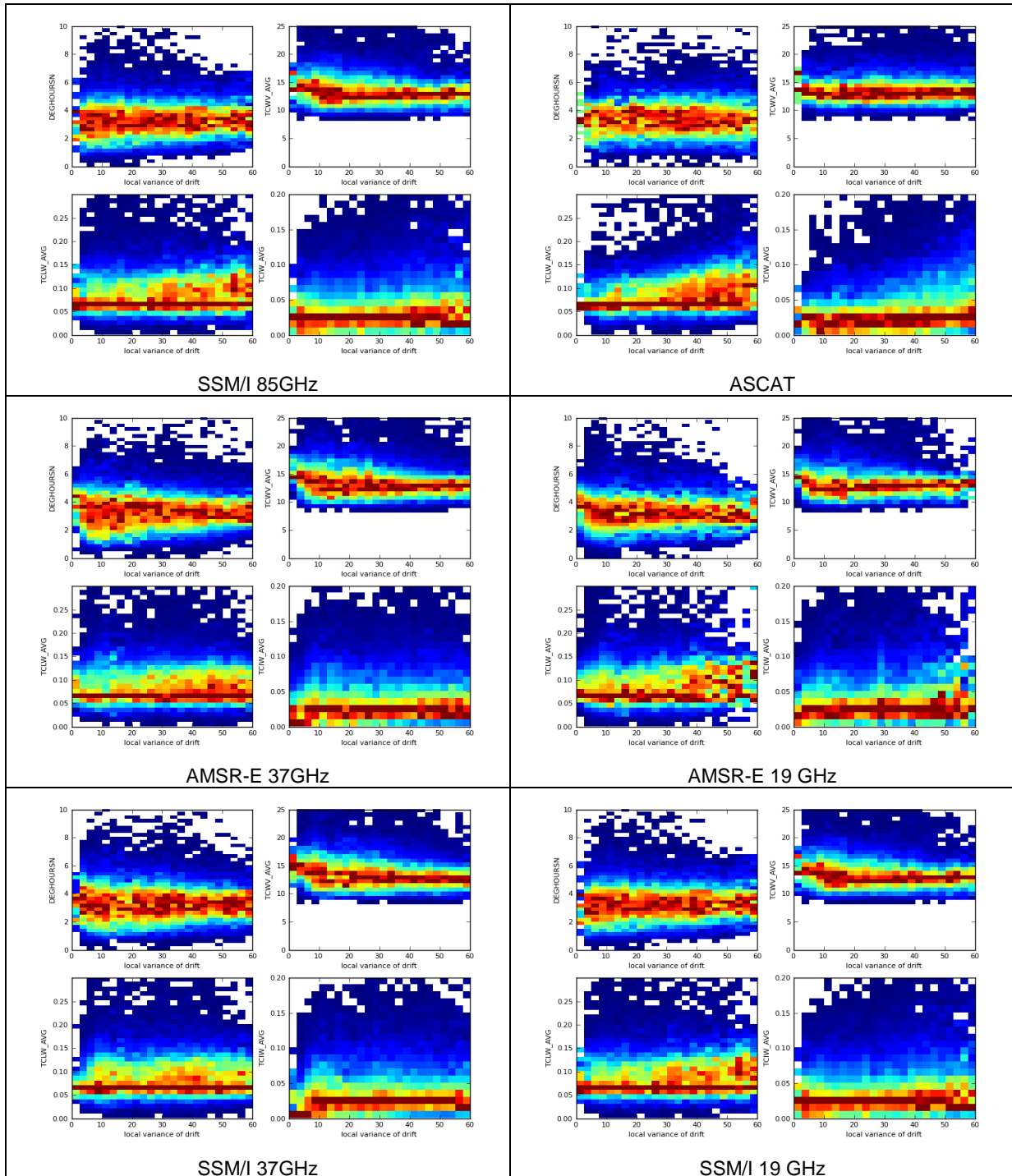

Figure 17: Same as previous for June
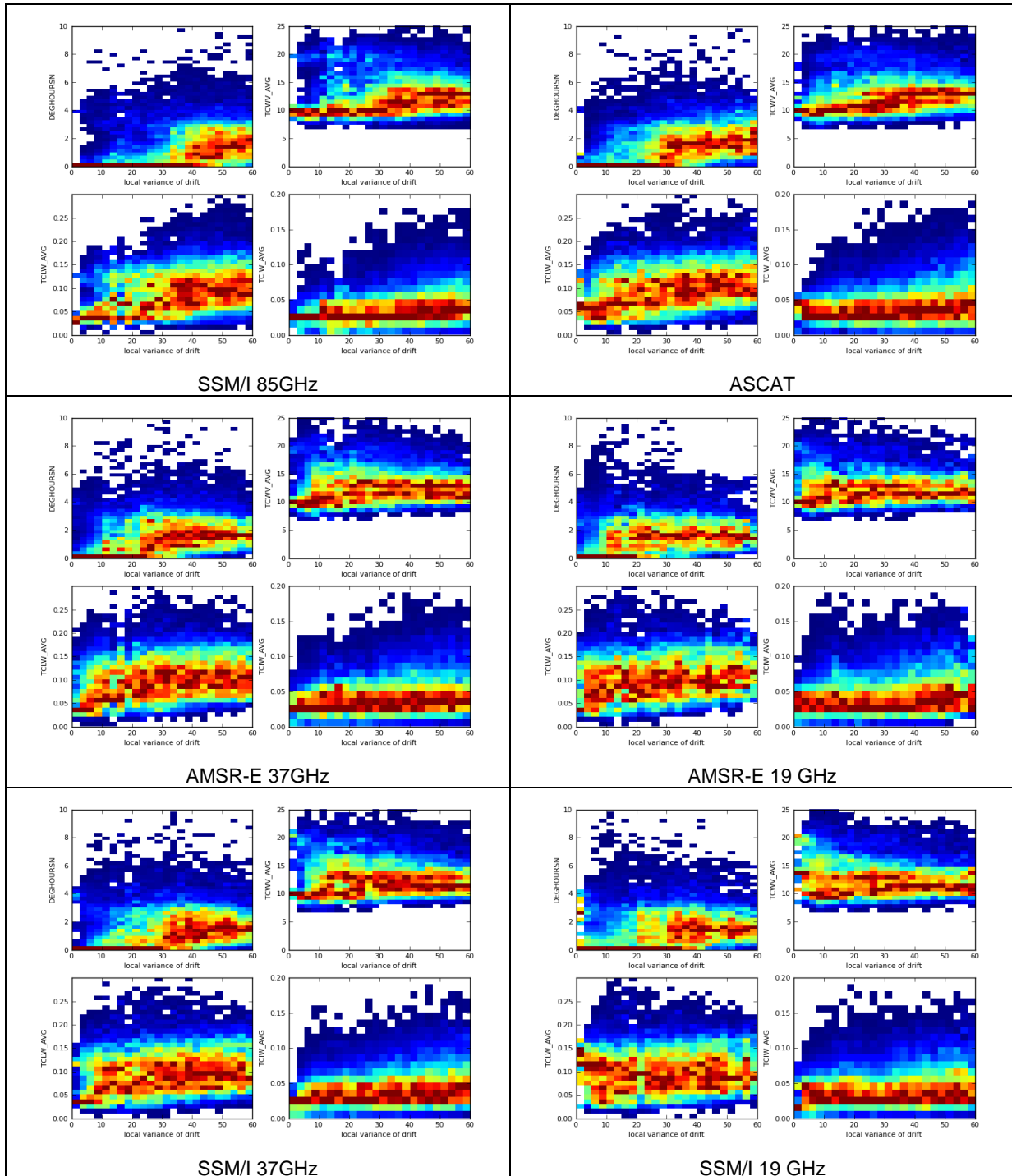
July 2008

Figure 18: Same as previous for July

August 2008

Figure 19: Same as previous for August

Deliverable report: D1.24 – Integrate additional satellite
sensors into daily ice drift map production to improve
summer (melt season) accuracy
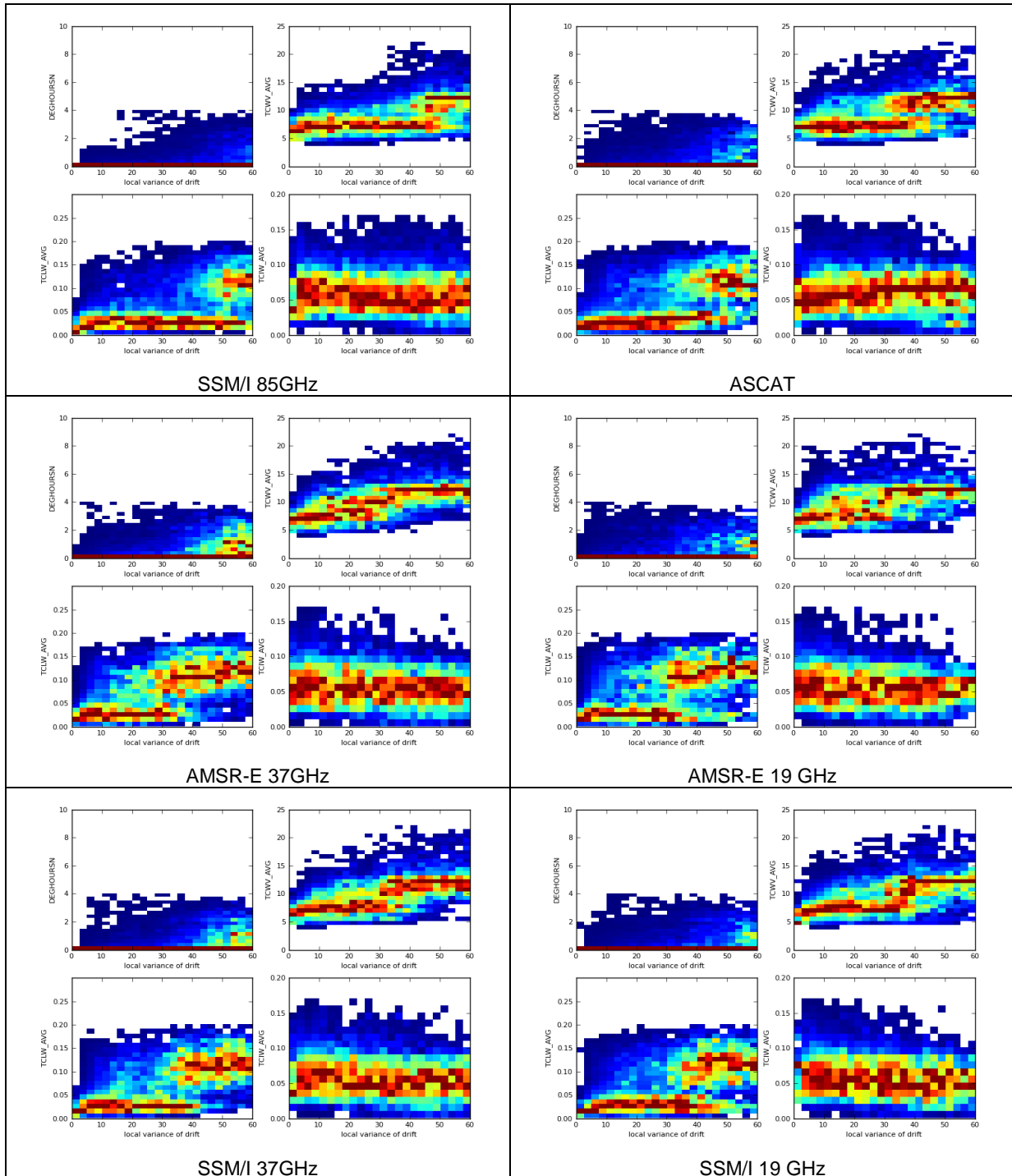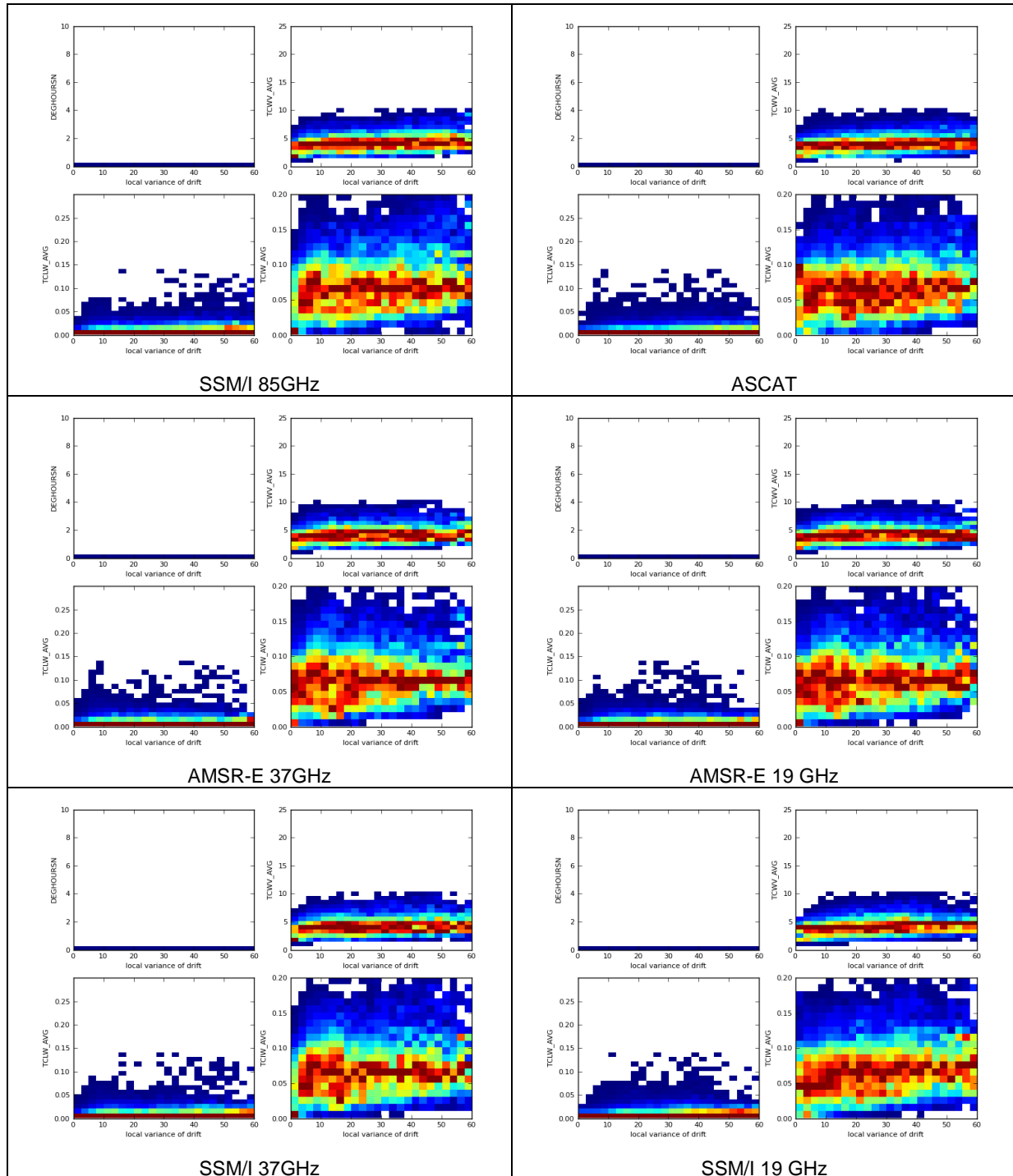
September 2008

Figure 20: Same as previous but September

October 2008

Figure 21: Same as previous for October